Unleashing Phosphorus Mononitride: Formation of PN-Multiple Bonded Exemplars $[NPS_2]^{2-}$, $[NPCl]^-$, and $[PN_4]^-$

Simon Edin,[1] Christian Sandoval-Pauker,[2] Nathan Yutronkie,[3] Zoltan Takacs,[1] Fabrice Wilhelm,[3] Andrei Rogalev,[3] Balazs Pinter,[2,4] Kasper S. Pedersen,[5,*] Anders Reinholdt[1,*]

The interstellar diatomic molecule, phosphorus mononitride (P≡N), is highly unstable under conditions typical on Earth, and its utility for constructing elusive P–N multiply-bonded archetypes is essentially uncharted. Herein, we show how Na(OCP) transfers a P atom to an electrophilic osmium nitride complex to form a terminally bound P≡N functionality. Quantum chemical calculations and X-ray absorption spectroscopy unveil a cumulenic [Os^{IV}=N=P] electronic structure comprising orthogonal Os=N and N=P π-bonding. The highly reduced P≡N ligand, formally $[PN]^{2-}$, undergoes two-fold oxidation with elemental sulfur to form a trigonal planar $[NPS_2]^{2-}$ group. On reaction with Ph_3CCl, the P≡N ligand forms a bent $[NPCl]^-$ motif coordinated to Os^{III} (S = ½). [3+2] cycloaddition of this radical species with Me_3SiN_3 forms an aromatic heterocyclic interpnictide, $[PN_4]^-$, that is inaccessible from the parent P≡N system.

Phosphorus mononitride (P≡N) was the first phosphorus-containing molecule to be identified in the interstellar medium, following Turner, Bally, and Ziurys's observations of its rotational lines from the Orion KL Nebula in 1987.[1,2] In our Solar System, P≡N has been detected in outgassing vapor from a comet, suggesting the diatomic molecule may have been a prebiotic source of phosphorus on the early Earth.[3] The first example of man-made P≡N was reported by Herzberg in 1933; an electric discharge through a tube containing N_2 and P_4 generated the diatomic molecule in the gas phase, as authenticated from 24 rotational bands.[4] Given its vulnerable triple bond,[5] studies of P≡N in condensed phase are far from trivial. Examples involve thermal decomposition of P_3N_5 at 800–900 °C followed by isolation in solid Kr,[6] dehalogenation of $[N_3P_3Cl_6]$ with Ag at 1300 K followed by isolation in solid Ar,[5] or photolysis of $[\{1,2\text{-}C_6H_4O_2\}P(N_3)]$ in solid Ar.[7] Even in cryogenic noble gas matrices, P≡N is unstable when the temperature rises above 10 K, which leads to oligomerization into discrete $[P_3N_3]$ species,[5,8,9] followed by the onset of higher polymerization products. To date, the smallest $[P_xN_y]$ molecule isolated under ambient conditions is Klapötke's azido-phosphazene, $[P_3(\mu\text{-}N)_3(N_3)_6]$;[10] a smaller system such as $P(N_3)_3$ decomposes rapidly in solution.[11]

An attractive strategy for studying P≡N is to form an adduct that stabilizes this reactive functionality. Thus, in 1988, Niecke and co-workers reported aryl cations $[Ar–N{\equiv}P]^+$ (**Chart 1, A**),[12,13] which display P≡N bond distances (1.475(8)–1.493(12) Å) similar to free, gaseous P≡N (1.49086(2) Å).[14] Later, research teams led by Bertrand,[15] Cummins,[16] and Schulz[17] demonstrated how P≡N could be sandwiched between carbenes (**B**), anthracene (**C**), or cyclobutadienes (**D**). The long P–N bonds (>1.69 Å) in these neutral species conform more closely to a description as P–N single-bonds than P≡N triple bonds. Given that P≡N is valence-shell isoelectronic to N_2, the heterodiatomic molecule could serve as a π-backbonding ligand in a transition metal complex. Initial studies by Cummins and co-workers revealed low stability of the transient complex $[\{Ar[^tBu]N\}_3V–N{\equiv}P]$, which oligomerizes to diphosphene and *cyclo*-triphosphane derivatives (Ar = 3,5-$Me_2C_6H_3$).[18] In 2020, Smith and co-workers isolated the first transition metal P≡N complexes by reductively coupling Fe^{IV} nitride and Mo^{VI} phosphide precursors to afford a heterobimetallic system, [Mo–PN–Fe]. Subsequent conversion of this complex with ^{t}BuNC yielded a P≡N complex anion, $[\{N(CH_2CH_2NSiMe_3)_3\}Mo–P{\equiv}N]^-$ (**E**) with an iron-isonitrile complex as counter ion; in the solid state, **E** converts photolytically to its N-bound linkage isomer.[19] More recently, Cummins and co-workers thermolyzed an anthracene-scaffolded azidophosphine, $[\{C_{14}H_{10}\}P(N_3)]$, to form anthracene, N_2, and P≡N; the heterodiatomic molecule was intercepted by a Fe^{II} complex (**F**).[20]

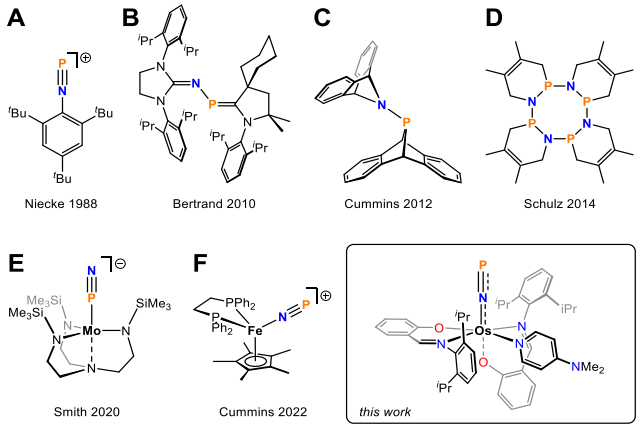

Chart 1. PN-containing molecules and metal complexes.

[1] Department of Chemistry, Lund University, 22100 Lund, Sweden, e-mail: anders.reinholdt@chem.lu.se
[2] Department of Chemistry and Biochemistry, University of Texas at El Paso, El Paso, TX 79968, USA
[3] ESRF-The European Synchrotron, CS 40220, 38043 Grenoble Cedex 9, France
[4] Current affiliation: European Research Council Executive Agency
[5] Department of Chemistry, Technical University of Denmark, Kemitorvet, DK-2800 Kgs. Lyngby, Denmark, e-mail: kastp@kemi.dtu.dk

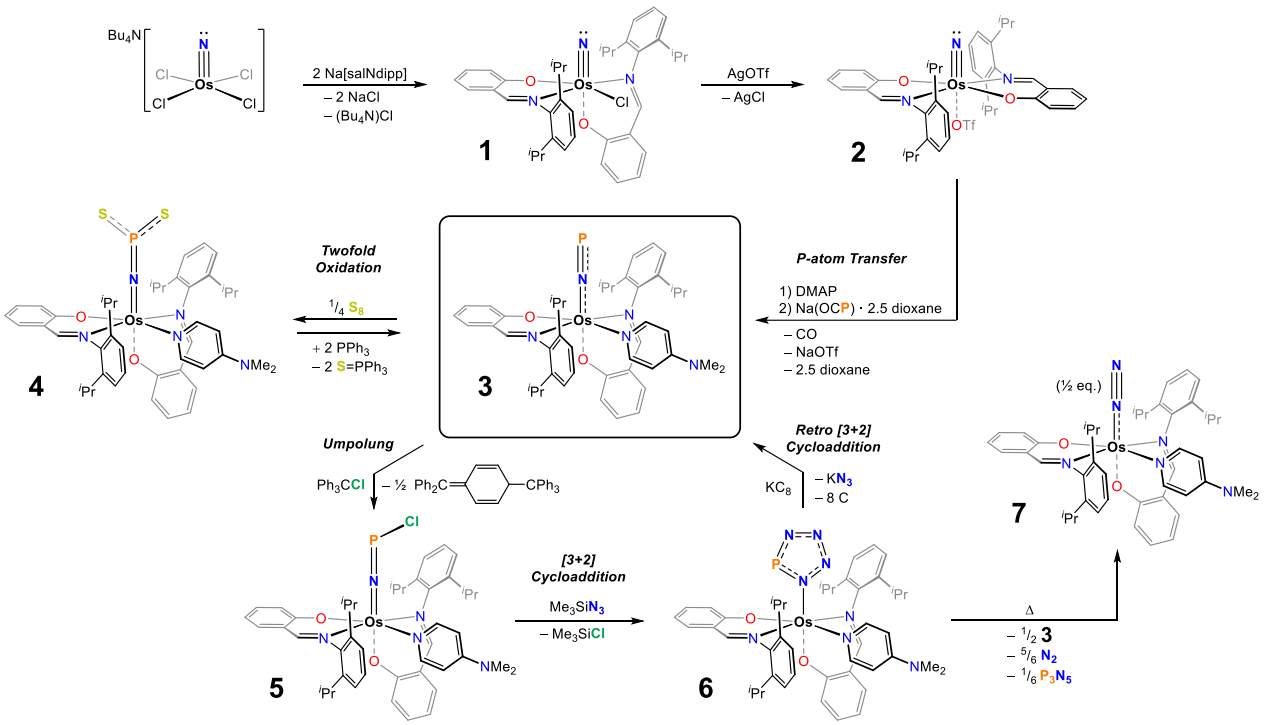

Scheme 1. Conversion of $(Bu_4N)[Os(N)Cl_4]$ to nitride precursors **1** and **2**. Treatment of **2** with DMAP and Na(OCP) yields P≡N complex **3**. Oxidation of **3** with S_8 and Ph_3CCl generates $[NPS_2]^{2-}$ complex **4** and $[NPCl]^-$ complex **5**, respectively. Complex **5** reacts with Me_3SiN_3 to form $[PN_4]^-$ complex **6**, which decomposes thermally to **3** and N_2 complex **7**.

The advanced synthetic protocols devised for making P≡N complexes have limited the utility of this functionality for constructing synthetically demanding phosphorus-nitrogen multiple bonded architectures by redox, atom transfer, or cycloaddition strategies. The only reported reactions of a P≡N ligand involve complex **E**, which can be metallated by a Rh^I center or silylated by Me_3SiCl.[19] These conversions bear a striking resemblance to metallation and silylation of transition metal dinitrogen complexes,[21] which calls into question whether N≡N and P≡N ligands display essentially identical reactivity. Given the elusive nature and uncharted reactivity of P≡N complexes, we sought alternative synthetic methodology toward this functionality and its chemistry. Herein, we describe how sodium phosphaethynolate delivers a P atom to an electrophilic osmium nitride complex to form a neutral [Os–N≡P] ↔ [Os=N=P] motif. We probe its electronic structure by isotopic labeling, multinuclear NMR, vibrational spectroscopy, X-ray absorption near edge structure (XANES) spectroscopy, and theoretical studies. We also report how the P≡N ligand can be elaborated into unique inorganic motifs such as a trigonal planar $[NPS_2]^{2-}$ and bent a $[NPCl]^-$ group. The P≡N ligand does not react directly with azides to form an aromatic heterocycle, $[PN_4]^-$, but is activated toward such [3+2] cycloaddition when subjected to *umpolung*.

Results and Discussion

P-Atom Transfer from Na(OCP) to an Osmium Nitride to Form a P≡N Complex (3). In spite of the high electronegativity of nitrogen (3.04, Pauling scale), high-valent, late transition metal nitride complexes possess such low d-orbital energies that their M≡N bonds may become polarized toward the metal center rather than the nitride ligand.[22] Given that group 8 nitrides react with elemental sulfur to form thionitrosyl complexes, [M–N≡S],[23-25] and considering the isoelectronic relationship between S and P^-, we inquired whether a P≡N ligand could be assembled from a terminal osmium nitride functionality and a phosphorus atom transfer reagent such as Na(OCP).[26,27] To this end, we treated nitride complex $(Bu_4N)[Os(N)Cl_4]$ with salicylaldimine ligand Na[salNdipp] in THF to form $[(salNdipp)_2(Cl)Os{\equiv}N]$ (**1**, **Scheme 1**, sal = salicylidene, dipp = 2,6-diisopropylphenyl). Further conversion of **1** with AgOTf afforded triflate complex $[(salNdipp)_2(OTf)Os{\equiv}N]$ (**2**) as orange crystals in 95% isolated yield after removal of AgCl. Treatment of **2** with Na(OCP) · 2.5 dioxane in THF led to several strong IR absorptions (1897–2202 cm^{-1}, suggesting coordinated CO ligand) as well as two ^{31}P NMR singlets (233, 220 ppm). To obtain a cleaner conversion, we first blocked one coordination site on the osmium center by treating **2** with 4-dimethylaminopyridine (DMAP) and subsequently with Na(OCP) · 2.5 dioxane in THF. This led to effervescence over 5 minutes and a color change from light to dark orange. Very dark (almost black) crystals of $[(salNdipp)_2(DMAP)Os(NP)]$ (**3**) were isolated in 94% yield after removal of NaOTf. X-ray crystallography revealed $salNdipp^-$ ligands arranged with the imine nitrogen atoms in a *trans*-configuration, the phenolate oxygen atoms *cis*, and DMAP coordinated *cis* to the P≡N ligand (**Figure 1A**). The phosphorus mononitride ligand displays linear coordination through nitrogen and a short P≡N bond, 1.536(5) Å, (elongated 3.0% relative to free P≡N).[14] Remarkably, the Os–NP bond, 1.846(5) Å, is shorter than any Os–N_2 bond in a dinitrogen complex (shortest: 1.896(6) Å).[28] As a direct comparison to **3**, we independently synthesized the N_2 analog, $[(salNdipp)_2(DMAP)Os(N_2)]$ (**7**), *vide infra*. The Os–N_2 bond in **7**, 1.903(6) Å, is substantially longer than the Os–NP bond in **3**, which suggests P≡N to be a stronger π-acid than its homoatomic analog.

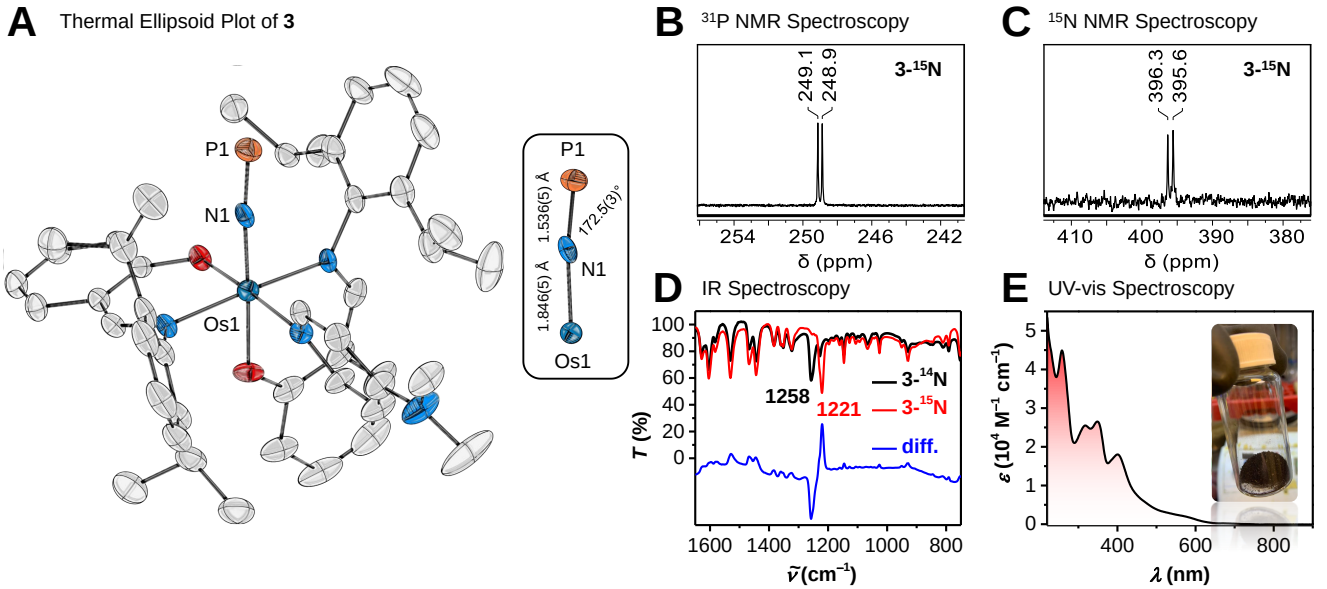

Figure 1. A: Molecular structure of P≡N complex **3** (50% probability; H atoms and toluene omitted). **B:** ^{31}P NMR data (**3-^{15}N**). **C:** ^{15}N NMR data (**3-^{15}N**). **D:** IR data (**3-^{14}N**, **3-^{15}N**). **E:** UV-vis data; inset shows crystals of **3**.

Spectroscopic Characterization of 3. To glean more information about the electronic structure of **3**, we turned to spectroscopic methods. ^{31}P NMR spectroscopy revealed a singlet at 249 ppm, evincing a shielded phosphorus nucleus compared to P≡N complexes **E** (312 ppm) and **F** (272 ppm) in **Chart 1**. An isotopically labelled sample of [(salNdipp)$_2$(DMAP)Os(^{15}NP)] (**3-^{15}N**), displayed a ^{15}N NMR doublet at 396 ppm ($^1J_{NP}$ = 62 Hz, **Figures 1B–1C**). The nitrogen nucleus is more shielded than its counterparts in **E** (445 ppm) and **F** (450 ppm). Turning to IR spectroscopy, **3** and **3-^{15}N** display P≡N stretching frequencies at 1258 and 1221 cm^{-1}, respectively (**Figure 1D**). These vibrations are redshifted relative to free P≡N (1323 cm^{-1}), indicating weakened P≡N bonding upon complexation.[6,29] Within the harmonic oscillator approximation, a ^{31}P^{14}N/^{31}P^{15}N isotopic system would shift from 1258 to 1229 cm^{-1} upon labeling, whereas an ^{190}Os^{14}N/^{190}Os^{15}N system would shift as low as 1218 cm^{-1}; clearly, **3**/**3-^{15}N** fall in between these limiting cases. For comparison, complex **F** displays less redshifted stretching vibrations (1271/1238 cm^{-1} for ^{14}N/^{15}N). Overall, the lower IR stretching mode and the more shielded ^{31}P and ^{15}N nuclei suggest that the P≡N ligand in **3** engages in more extensive π-backbonding with the π-basic Os^{II} center, as compared to previously reported Mo^{II} and Fe^{II} complexes **E** and **F**. Finally, UV-vis spectroscopy revealed intense absorptions at 258, 318, 348, and 401 nm (ε = 45000, 26000, 27000, and 18000 M^{-1} cm^{-1}, respectively), indicative of charge-transfer transitions between the Os center and the P≡N ligand (**Figure 1E**).

Electronic Structure of 3. We further studied the electronic structure of **3** by density functional theory (DFT), using PBE0/def2-TZVP(-f) for geometry optimizations and TPSSh/def2-TZVP for single-point calculations. In theory, **3** can be described by three limiting resonance contributors, namely [Os^{II}] singly bonded to a neutral [P≡N] ligand, [Os^{IV}] doubly bonded to a dianionic [P=N]$^{2-}$ ligand, or [Os^{VI}] triply bonded to a tetraanionic [P–N]$^{4-}$ ligand. Upon reaction with a hypothetical electrophile, these scenarios could lead to single (E_1), twofold (E_2), or threefold (E_3) functionalization of the P≡N ligand (**Figure 2A**). In a molecular orbital depiction, an [OsNP] fragment possesses 5d$_{xz}$, 5d$_{yz}$, 2p$_x$, 2p$_y$, 3p$_x$, and 3p$_y$ atomic orbitals aligned for π-bonding (**Figure 2B**), yielding linear combinations that are in-phase bonding (π), nonbonding with a nodal plane at N (π_{nb}), and out-of-phase antibonding (π*). Calculated molecular orbitals for **3** (**Figure 2C**) unambiguously show the two π-systems corresponding to the in-phase bonding π set; however, the unsymmetrical ligand field around osmium concentrates HOMO–23 at N–P, whereas HOMO–20 is Os–N centered. These localized and orthogonal N=P and Os=N π-bonds suggest that **3** possesses a dominant cumulenic character, [Os=N=P]; strong π-backdonation from osmium confers an [N=P]$^{2-}$ character on the diatomic ligand. Looking to higher energy, the π_{nb} orbitals (HOMO–2, HOMO) have large amplitudes on Os and P, with a nodal plane on the central N atom. Interpreted as Lewis structures, the π_{nb} orbitals represent two d-electrons on Os and one lone pair on P. Concomitant with this notion, electrophilic Fukui functions display large amplitudes on Os and P (**SI, Figure S9.2.1**), pointing out likely loci of electrophilic functionalization (*vide infra*). Finally, the out-of-phase π* set is, as expected, energetically low-lying virtual orbitals (LUMO+2 and LUMO+3).

In harmony with the topology of the π and π_{nb} molecular orbitals, Mayer bond orders (**Figure 2D**) also indicate multiple bond character for both the N–P bond (2.22) and the Os–N bond (1.21), suggesting a dominant [Os=N=P] Lewis structure. Topological analysis using quantum theory of atoms in molecules (QTAIM) reveals moderate ellipticity (ε = 0.100) for the Os=N bond, supporting a nonsymmetric electron distribution within this π-bond, whereas the N=P bond is closer to cylindrical symmetry (ε = 0.010). When comparing the electronic structure of **3** to the few reported P≡N systems (**Chart 1**), both **E** and **F** display very marginal π-backbonding and are best represented by P≡N triple bonds.[19,20] In line with this bonding scheme, Smith showcased how silylation and metallation led to linear [Mo–P≡N–X] motifs (X = SiMe$_3$, Rh^I), indicating E_1 reactivity in **Figure 2A**. Conforming more

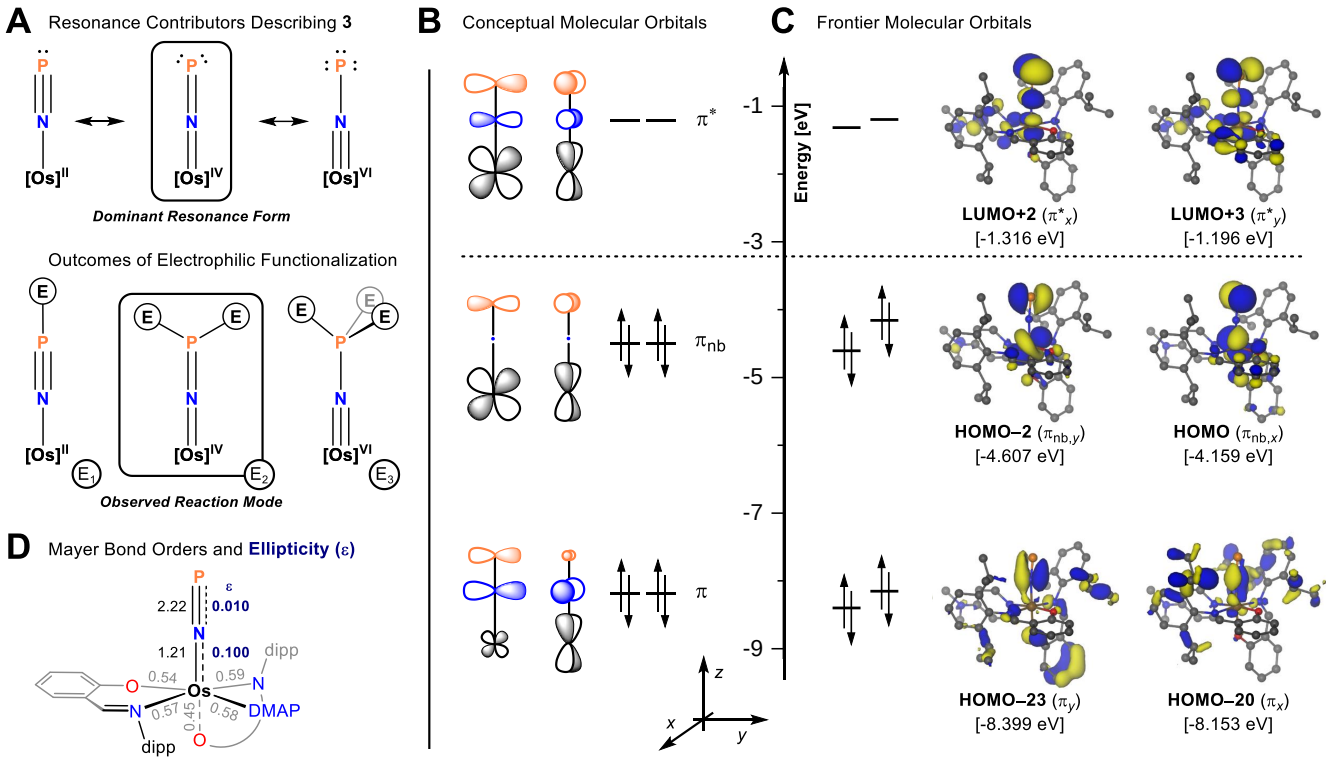

Figure 2. A: Possible resonance contributors and products expected from electrophilic functionalization of **3**. **B:** Conceptual π molecular orbitals. **C:** Frontier molecular orbitals from DFT. **D:** Mayer bond orders and bond ellipticities.

closely to an [Os=N=P] description, **3** could conceivably undergo twofold electrophilic functionalization in line with E_2 reactivity.

Oxidation of 3 by Sulfur to Form an $[NPS_2]^{2-}$ Ligand. To probe the reactivity of the osmium-coordinated P≡N ligand, we treated **3** with elemental sulfur. Considering **Figure 2A**, this could generate unprecedented ternary ions such as $[NPS_2]^{2-}$ or $[NPS_3]^{4-}$ or a heavy-atom analog of nitrous oxide, NPS.[30] When using ¼ eq. S_8, diamagnetic [(salNdipp)$_2$(DMAP)Os(NPS$_2$)] (**4**) formed in 73% yield as dark orange crystals. Desulfurization with PPh_3 regenerated **3** along with Ph_3PS. X-ray crystallography revealed an osmium center bound to a trigonal planar nitridodisulfidophosphate(V) ligand, $[NPS_2]^{2-}$, coordinated linearly through N (**Figure 3A**). The planar P^V center (angle sum 359.8°) contrasts with the pyramidalized P^{III} center (311.9°) in the known complex, [{Ar[^{t}Bu]N}$_3$V–{NPS$_2$(C$_{10}$H$_6$)}], formed by trapping transient [{Ar[^{t}Bu]N}$_3$V^{III}–N≡P] with 1,8-naphthalenediyl disulfide ($C_{10}H_6)S_2$.[18] The Os–N, P–N, and P–S bond distances in **4** indicate π-delocalization in the [OsNPS$_2$] fragment, which is corroborated by Mayer bond orders (1.30–1.67). The formation of **4** upon E_2-type reactivity (**Figure 2A**) demonstrates the striking contrast in reactivity of **3** compared to the few P≡N complexes reported to date. Spectroscopically, **4** displays a ^{31}P NMR singlet at a lower chemical shift than **3** (233 ppm). A ^{1}H-^{15}N HMBC experiment revealed eight long-range correlations ($^4J_{HN}$, $^6J_{HN}$, $^7J_{HN}$) to the $[NPS_2]^{2-}$ ligand, unequivocally identifying a low-intensity and strongly deshielded ^{15}N doublet at 955 ppm ($^1J_{NP}$ = 51 Hz, **Figure 3A**).

Chlorination of 3 to Form an $[NPCl]^-$ Ligand. To test for radical reactivity, we treated **3** with trityl chloride. This generated Gomberg's dimer (observed by ^{1}H NMR) and a mono-chlorinated Os^{III} product [(salNdipp)$_2$(DMAP)Os(NPCl)] (**5**), isolated as dark orange crystals in 97% yield. Excess trityl chloride did not perturb the product distribution. The $[NPCl]^-$ ligand is the isoelectronic phosphorus analog of the rare main group terminal nitride, thiazyl chloride, [NSCl].[31] X-ray crystallography revealed linear Os–N–P and bent N–P–Cl geometries, in line with a lone pair on phosphorus (**Figure 3B**). Interestingly, **5** possesses one of the longest structurally characterized P–Cl bonds (top 1%), suggesting a labile halogen substituent. Given its radical nature, **5** displays paramagnetically shifted ^{1}H NMR resonances from −22 to +23 ppm (FWHM 5–1100 Hz). Magnetization measurements (**Figure 3B**) revealed an effective magnetic moment (μ_{eff} = 1.64 μ_B, 300 K) in accord with the spin-only value for an effective S = ½ system. The magnetic moment remains practically constant until 20 K but increases slightly at the lowest temperature to reach 1.74 μ_B at 3 K, suggesting the presence of weak ferromagnetic interactions between the constituent molecules. All magnetic field and low-temperature magnetization data collapse on a single curve when plotted against the reduced variable $\mu_0 HT^{-1}$, which is well described by an effective S = 1/2 Brillouin function with g = 1.91(5) (**Figure 3B**, inset). The significant reduction of g from 2.0 suggests a dominant metallo-radical character of **5**. In accord, computed Löwdin spin densities (**SI, Figure S9.2.2**) indicate an Os^{III}-centered radical with minor spin delocalization onto the nitrogen of $[NPCl]^-$.

[3+2] Cycloaddition of 5 with Azide. In spite of the hypothetical triple bond reactivity of a P≡N ligand, **3** does not undergo [3+2] cycloaddition with azides to form a $[PN_4]^-$ heterocycle. However, the oxidized species, **5**, offers a P≡N fragment subjected to *umpolung*, and upon

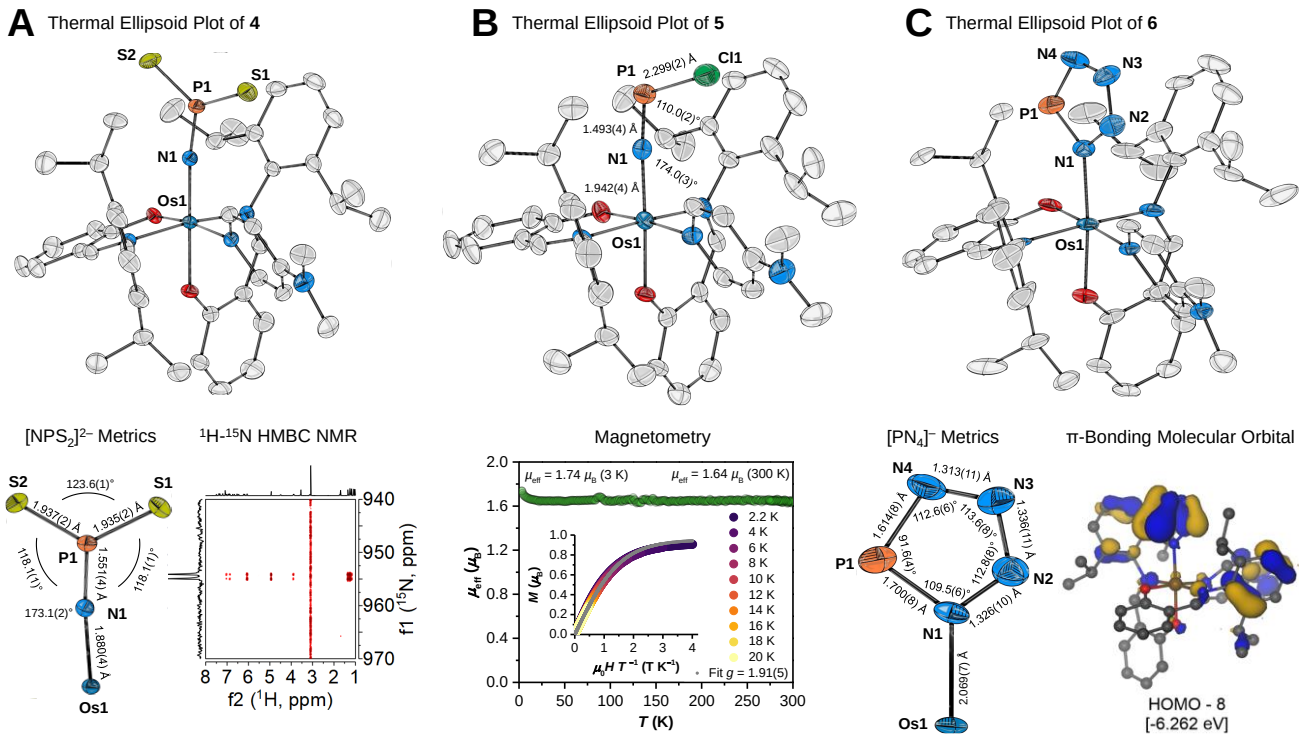

Figure 3. A: Top, X-ray structure of **4** (50% probability; H atoms, toluene omitted). Bottom, $[NPS_2]^{2-}$ metrics (left), ^1H-^{15}N HMBC data (right). **B:** Top, X-ray structure of **5** (50% probability; H atoms, hexane omitted). Bottom, effective magnetic moment (μ_{eff}) at 3–300 K, inset, magnetic field dependence of the magnetization, *M versus* $\mu_0 HT^{-1}$ (including a fit to the S = 1/2 Brillouin function). **C:** Top, X-ray structure of **6** (50% probability; H atoms, hexane omitted). Bottom, $[PN_4]^-$ metrics (left), one of the π-bonding molecular orbitals of **4** illustrating its aromatic character (right).

reaction with Me_3SiN_3, a thermally sensitive tetrazaphospholide Os^{III} complex, [(salNdipp)$_2$(DMAP)Os(η^1-N_4P)] (**6**), forms as orange crystals in 55% yield. Aromatic pnictogen rings, and nitrogen-rich interpnictides in particular, are challenging constructs. Baudler and co-workers reported $[P_5]^-$ in 1987,[32] but it was not until 2016 and 2017, that Velian and Cummins isolated the first unsubstituted $[P_2N_3]^-$ heterocycle,[33] and Lu and co-workers isolated $[N_5]^-$, respectively.[34,35] All other unsubstituted $[P_nN_{n-5}]^-$ rings have remained unknown.[36,37] X-ray crystallography identified **6** as a single linkage isomer with a planar $[PN_4]^-$ ring coordinated through a nitrogen adjacent to phosphorus (**Figure 3C**). The N–N bonds are alike within 0.02 Å, while the two P–N bonds differ by almost 0.1 Å. Bond angles around the nitrogen atoms lie fairly close to the value for a regular pentagon, whereas the P–N bonds are practically orthogonal. The Os–N_4P bond distance is alike the other Os–$N_{imine/DMAP}$ bonds of **6**, indicating coordination through a dative σ-bond. Computational analysis revealed π-delocalization within the $[PN_4]^-$ ring (**Figure 3C**) and Mayer bond orders spanning 1.12–1.49, in line with an aromatic character, as well as an Os^{III}-centered radical (**SI, Figure S9.2.3**). Being paramagnetic, **6** displays broad ^1H NMR resonances from −30 to +19 ppm (FWHM 10–1500 Hz) and a magnetic moment of 1.85 μ_B in solution (Evans' method, THF, 298 K). Thermal decomposition of **6** (room temperature) generates an 1:1 mixture of **3** and dinitrogen complex [(salNdipp)$_2$(DMAP)Os(N_2)] (**7**), along with a white solid, attributable to binary phosphorus(V) nitrogen species.[38] The N_2 complex could be separated after selectively converting **3** into **4** with S_8. The metastable nature of **6** is also manifested in its reduction chemistry; treatment with KC_8 does not produce a hypothetical salt such as "[K][(salNdipp)$_2$(DMAP)Os(η^1-N_4P)]", but instead leads to a clean retro [3+2] cycloaddition, forming **3** and KN_3 (identified by ^1H/^{31}P NMR and IR data, $\upsilon_{N_3^-}$ = 2012 cm^{-1}).

X-ray Spectroscopic Studies. To gain element-specific information about the electronic structure of **2**, **3**, **4**, and **5**, we turned to X-ray absorption near edge structure (XANES) spectroscopy. For the phosphorus *K*-edge (**Figure 4A**), the dipole selection rule $\Delta l = \pm 1$ allows excitations from filled core 1s levels to vacant valence orbitals having 3p character. Complexes **3**, **4**, and **5** display drastic spectral differences, which are brought about by a subtle interplay between the oxidation state of phosphorus, covalent orbital interactions with neighboring atoms, and the local geometry about the phosphorus atom.[39] These spectral features directly map the profound differences in electronic structure for the P≡N, $[NPS_2]^{2-}$, and $[NPCl]^-$ ligands. We also recorded osmium $L_{2,3}$ XANES to probe directly the electronic configuration of the 5d orbitals of osmium (**Figure 4B**). The spectra show strong resonances (white lines) at the absorption edges, corresponding to dipole-allowed $2p_{1/2,\,3/2} \rightarrow 5d_{3/2,\,5/2}$ transitions. Of the series of compounds, **2** features the highest white line photon energies, which are slightly higher than for both **3** and **4**. The lowest photon energies are observed for **5** commensurate with the lower, formal oxidation state assignment. In addition, the white line integrals are a sensitive measure of the number of electron holes in the Os 5d states (**Figure 4C**), as previously reported.[40,41] By applying the spin-orbit sum rules for p→d transitions,[42] the number of electrons populating the $5d_{5/2}$ and $5d_{3/2}$ sublevels (n_e) were quantitatively determined. This, in

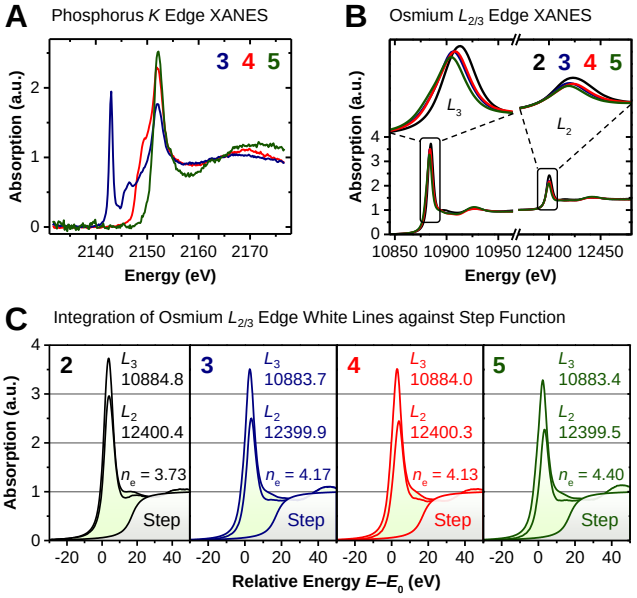

Figure 4. XANES spectral studies. **A:** Phosphorus *K*-edge (**3**, **4**, **5**). **B:** Osmium L_3 and L_2 edge (**2**, **3**, **4**, **5**). **C:** Peak energies [eV] and integrals of osmium $L_{2/3}$ white lines (See Experimental Section) along with 5d-orbital populations (n_e) as estimated from the spin-orbit sum rules.

congruence with the energy positions of the white lines, confirms the highest oxidation state in **2** (n_e = 3.73; formally Os^{VI}), a common, intermediate oxidation state in **3** and **4** (n_e = 4.17 and 4.13; formally Os^{IV}), and the lowest oxidation state in **5** (n_e = 4.40; formally Os^{III}). Bear in mind that the present analysis does not provide the true oxidation state since any contributions arising from transitions to the 6s and 6p states are neglected. The spectroscopic findings can be well understood in terms of ligand-centered oxidations of a $[PN]^{2-}$ moiety, forming closed-shell motifs, $[NPS_2]^{2-}$, and $[NPCl]^-$, engaged in cumulenic bonding with osmium. Remarkably, as evidenced from XANES spectroscopy, oxidation of **3** to **4** leaves the oxidation state of osmium invariant, whereas oxidation of **3** to **5** leads to a lower oxidation state of osmium.

Conclusions

The interstellar diatomic molecule, phosphorus mononitride (P≡N), offers singular access to phosphorus-nitrogen multiple bonded constructs, serving as exemplars in structure, bonding, and reactivity. Only a few synthetic strategies to stabilize P≡N have been reported. We have demonstrated how P-atom transfer from Na(OCP) to an osmium nitride assembles a terminally bound P≡N ligand, (**3**). Theoretical modeling coupled with XANES spectroscopy revealed a highly reduced P≡N functionality, formally $[PN]^{2-}$, and a cumulenic $[Os^{IV}=N=P]$ electronic structure with orthogonal Os=N and N=P π-bonding. The P≡N ligand, being both coordinatively stabilized and reductively activated by the π-basic osmium scaffold, undergoes oxidative conversions into unique binary and ternary π-bonded motifs, including trigonal planar $[NPS_2]^{2-}$ (**4**), bent $[NPCl]^-$ (**5**), and cyclic $[PN_4]^-$ (**6**); we are presently extending this strategy to other coordinated intermediates that cannot be accessed through classic synthetic chemistry.

References

1 Turner, B. E. & Bally, J. Detection of Interstellar PN: The First Identified Phosphorus Compound in the Interstellar Medium. *Astrophys. J.* **321**, L75-L79 (1987).
2 Ziurys, L. M. Detection of Interstellar PN: The First Phosphorus-bearing Species Observed in Molecular Clouds. *Astrophys. J.* **321**, L81 (1987).
3 Rivilla, V. M., *et al.* ALMA and ROSINA detections of phosphorus-bearing molecules: the interstellar thread between star-forming regions and comets. *Mon. Not. R. Astron. Soc.* **492**, 1180-1198 (2020).
4 Curry, J., Herzberg, L. & Herzberg, G. Spectroscopic Evidence for the Molecule PN. *J. Chem. Phys.* **1**, 749 (1933).
5 Ahlrichs, R., Bär, M., Plitt, H. S. & Schnöckel, H. The stability of PN and $(PN)_3$. Ab initio calculations and matrix infrared investigations. *Chem. Phys. Lett.* **161**, 179-184 (1989).
6 Atkins, R. M. & Timms, P. L. The matrix infrared spectrum of PN and SiS. *Spectrochim. Acta, Part A* **33**, 853-857 (1977).
7 Qian, W., Wende, R. C., Schreiner, P. R. & Mardyukov, A. Selective Preparation of Phosphorus Mononitride (P≡N) from Phosphinoazide and Reversible Oxidation to Phosphinonitrene. *Angew. Chem., Int. Ed.* **62**, e202300761 (2023).
8 Zhu, C., *et al.* The elusive cyclotriphosphazene molecule and its Dewar benzene–type valence isomer (P_3N_3). *Sci. Adv.* **6**, eaba6934 (2020).
9 Zhu, C., *et al.* Identification of a prismatic P_3N_3 molecule formed from electron irradiated phosphine-nitrogen ices. *Nat. Commun.* **12**, 5467 (2021).
10 Göbel, M., Karaghiosoff, K. & Klapötke, T. M. The First Structural Characterization of a Binary P–N Molecule: The Highly Energetic Compound P_3N_{21}. *Angew. Chem., Int. Ed.* **45**, 6037-6040 (2006).
11 Dillon, K. B., Platt, A. W. G. & Waddington, T. C. Reactions of alkali-metal azides with some halogenophosphorus compounds. *J. Chem. Soc., Dalton Trans.*, 1036-1041 (1980).
12 Niecke, E., Nieger, M. & Reichert, F. Arylmino(halogeno)phosphanes $XP=NC_6H_2tBu_3$ (X = Cl, Br, I) and the Iminophosphenium Tetrachloroaluminate $[P\equiv NC_6H_2tBu_3]^{\oplus}[AlCl_4]^{\ominus}$: the First Stable Compound with a PN Triple Bond. *Angew. Chem., Int. Ed. Engl.* **27**, 1715-1716 (1988).
13 Niecke, E., Nieger, M., Reichert, F. & Schoeller, W. W. Synthesis, Structure and Bonding in the Donor-Acceptor Complex $[tBu_2PSe_2]\cdot[PNAryl]$: En Route to the P≡N Bond. *Angew. Chem., Int. Ed. Engl.* **27**, 1713-1714 (1988).
14 Wyse, F. C., Manson, E. L. & Gordy, W. Millimeter Wave Rotational Spectrum and Molecular Constants of $^{31}P^{14}N$. *J. Chem. Phys.* **57**, 1106-1108 (1972).
15 Kinjo, R., Donnadieu, B. & Bertrand, G. Isolation of a Carbene-Stabilized Phosphorus Mononitride and Its Radical Cation ($PN^{+\cdot}$). *Angew. Chem., Int. Ed.* **49**, 5930-5933 (2010).
16 Velian, A. & Cummins, C. C. Facile Synthesis of Dibenzo-7λ^3-phosphanorbornadiene Derivatives Using Magnesium Anthracene. *J. Am. Chem. Soc.* **134**, 13978-13981 (2012).
17 Hering, C., Schulz, A. & Villinger, A. Diatomic PN – trapped in a *cyclo*-tetraphosphazene. *Chem. Sci.* **5**, 1064-1073 (2014).
18 Courtemanche, M.-A., Transue, W. J. & Cummins, C. C. Phosphinidene Reactivity of a Transient Vanadium P≡N Complex. *J. Am. Chem. Soc.* **138**, 16220-16223 (2016).
19 Martinez, J. L., *et al.* Stabilization of the Dinitrogen Analogue, Phosphorus Nitride. *ACS Cent. Sci.* **6**, 1572-1577 (2020).
20 Eckhardt, A. K., *et al.* Taming phosphorus mononitride. *Nat. Chem.* **14**, 928-934 (2022).
21 Peters, J. C., *et al.* Redox-Catalyzed Binding of Dinitrogen by Molybdenum *N-tert*-Hydrocarbylanilide Complexes: Implications for Dinitrogen Functionalization and Reductive Cleavage. *J. Am. Chem. Soc.* **121**, 10053-10067 (1999).
22 Smith, J. M. in *Progress in Inorganic Chemistry Volume 58* 417-470 (John Wiley & Sons Inc., 2014).
23 Mutoh, Y. in *Chalcogen Chemistry: Fundamentals and Applications* (eds Vito Lippolis, Claudio Santi, Eder J. Lenardão, & Antonio L. Braga) 27-57 (The Royal Society of Chemistry, 2023).
24 Crevier, T. J., Lovell, S., Mayer, J. M., Rheingold, A. L. & Guzei, I. A. Chalcogen Atom Transfer to a Metal Nitrido. The First

Transition Metal Selenonitrosyl Complex. *J. Am. Chem. Soc.* **120**, 6607-6608 (1998).
25 Ng, H.-Y., *et al.* Ruthenium(VI) nitrido complexes with a sterically bulky bidentate Schiff base ligand. *Inorg. Chim. Acta* **394**, 171-175 (2013).
26 Heift, D., Benkő, Z. & Grützmacher, H. Coulomb repulsion versus cycloaddition: formation of anionic four-membered rings from sodium phosphaethynolate, Na(OCP). *Dalton Trans.* **43**, 831-840 (2014).
27 Goicoechea, J. M. & Grützmacher, H. The Chemistry of the 2-Phosphaethynolate Anion. *Angew. Chem., Int. Ed.* **57**, 16968-16994 (2018).
28 Lee, J.-H., Pink, M., Tomaszewski, J., Fan, H. & Caulton, K. G. Facile Hydrogenation of N_2O by an Operationally Unsaturated Osmium Polyhydride. *J. Am. Chem. Soc.* **129**, 8706-8707 (2007).
29 Ahmad, I. K. & Hamilton, P. A. The Fourier Transform Infrared Spectrum of PN. *J. Mol. Spectrosc.* **169**, 286-291 (1995).
30 Zeng, X., Beckers, H., Willner, H. & Francisco, J. S. Experimental Observation of the 16-Electron Molecules SPN, SNP, and Cyclic PSN. *Angew. Chem., Int. Ed.* **51**, 3334-3339 (2012).
31 Patton, R. L. & Jolly, W. L. Sublimation of trithiazyl trichloride and the equilibrium between trithiazyl trichloride and thiazyl chloride. *Inorg. Chem.* **9**, 1079-1083 (1970).
32 Baudler, M., Düster, D. & Ouzounis, D. Beiträge zur Chemie des Phosphors. 172. Existenz und Charakterisierung des Pentaphosphacyclopentadienid-Anions, P_5^-, des Tetraphosphacyclopentadienid-Ions, P_4CH^-, und des Triphosphacyclobutenid-Ions, $P_3CH_2^-$. *Z. Anorg. Allg. Chem.* **544**, 87-94 (1987).
33 Velian, A. & Cummins, C. C. Synthesis and characterization of $P_2N_3^-$: An aromatic ion composed of phosphorus and nitrogen. *Science* **348**, 1001-1004 (2015).
34 Xu, Y., et al. A series of energetic metal pentazolate hydrates. *Nature* **549**, 78-81 (2017).
35 Zhang, C., Sun, C., Hu, B., Yu, C. & Lu, M. Synthesis and characterization of the pentazolate anion *cyclo*-N_5^- in $(N_5)_6(H_3O)_3(NH_4)_4Cl$. *Science* **355**, 374-376 (2017).
36 David, G., Niecke, E., Nieger, M., Gönna, V. V. D. & Schoeller, W. W. [*n* + 2]-Cycloadditionsreaktionen des (Arylimino)phosphenium-Ions, $[P{\equiv}NAr]^+$–kationische PN-Heterocyclen mit ungewöhnlicher Struktur und Bindungssituation. *Chem. Ber.* **126**, 1513-1517 (1993).
37 Villinger, A., Mayer, P. & Schulz, A. $GaCl_3$-assisted [2 + 3] cycloaddition: A route to tetrazaphospholes. *Chem. Commun.*, 1236-1238 (2006).
38 Schnick, W., Lücke, J. & Krumeich, F. Phosphorus Nitride P_3N_5 Synthesis, Spectroscopic, and Electron Microscopic Investigations. *Chem. Mater.* **8**, 281-286 (1996).
39 Donahue, C. M. & Daly, S. R. Ligand K-Edge XAS Studies of Metal-Phosphorus Bonds: Applications, Limitations, and Opportunities. *Comments Inorg. Chem.* **38**, 54-78 (2018).
40 Pedersen, K. S., *et al.* Iridates from the molecular side. *Nat. Commun.* **7**, 12195 (2016).
41 Pedersen, K. S., *et al.* $[OsF_6]^{x-}$: Molecular Models for Spin-Orbit Entangled Phenomena. *Chem. Eur. J.* **23**, 11244-11248 (2017).
42 van der Laan, G. & Thole, B. T. Local Probe for Spin-Orbit Interaction. *Phys. Rev. Lett.* **60**, 1977-1980 (1988).

Methods

All synthetic operations were performed in Vigor glove boxes under a purified atmosphere of N_2 (O_2 < 1 ppm, H_2O < 1 ppm). Hexane and toluene were initially purified with an MBraun SPS system. Tetrahydrofuran and diethyl ether were initially stored over sodium benzophenone ketyl diradical, distilled by trap-to-trap transfer *in vacuo*, and degassed by freeze-pump-thaw cycles. Benzene-d_6 and THF-d_8 were stored over a potassium mirror overnight, sublimed/distilled by trap-to-trap transfer *in vacuo*, and degassed by freeze-pump-thaw cycles. The water content of the solvents was further reduced by storage over 4 Å molecular sieves. Celite and 4 Å molecular sieves were activated *in vacuo* overnight at 175 °C.

Synthesis of [(salNdipp)$_2$(DMAP)Os(^{15}NP)] (3-^{15}N)

A solution of H(salNdipp) (116.2 mg, 0.413 mmol) in 3 ml THF was added over 5 minutes to a suspension of NaH (14.0 mg, 0.583 mmol, 1.4 eq) in 1 ml THF. Vigorous effervescence ensued (H_2, several minutes). The suspension was left to stir over 90 minutes, resulting in a slight darkening of the yellow color. Residual NaH was removed by filtration through celite, and the filtrate was transferred to a vial containing (Bu_4N)[Os(^{15}N)Cl_4] (121.0 mg, 0.205 mmol) and left to stir overnight, resulting in a slow color change from dark purple to orange. The solvent was removed under reduced pressure, and the residue was redissolved in a mixture of Et_2O and toluene (15 ml, 1:2, Et_2O:tol), filtered through celite (removing (Bu_4N)Cl and NaCl) and washed through the filter with 2×2 ml toluene. The solvent was removed under reduced pressure, leaving [(salNdipp)$_2$(Cl)Os^{15}N] (**1-^{15}N**) as an orange solid. The solid was redissolved in 5 ml THF, and a solution of AgOTf (53.8 mg, 0.209 mmol) in 3 ml toluene was added under vigorous stirring. After 30 minutes, the suspension was filtered through celite (removing AgCl), and the solvents were removed under reduced pressure, leaving [(salNdipp)$_2$(OTf)Os^{15}N] (**2-^{15}N**) as an orange crystalline material. The resulting solid and 4-(dimethylamino)pyridine (DMAP, 25.0 mg, 0.205 mmol) were dissolved in 15 ml toluene, and the reaction mixture was left to stir overnight, resulting in an orange suspension. The solvent was removed under reduced pressure. To the solid, Na(OCP) · 2.5 dioxane (68.9 mg, 0.228 mmol, 1.1 eq) in 5 ml THF was added, resulting in evolution of gas (CO, for several minutes) and a color change from light orange to very dark orange. After 30 minutes, the reaction mixture was filtered through celite, and the solvent was removed under reduced pressure. The solid was then redissolved in a minimal amount of toluene (ca. 30 ml), and Al_2O_3 (pH 7, 2.0 g) was added to adsorb NaOTf (this byproduct forms a THF adduct with similar solubility to **3**). The mixture was stirred for 2 hours, the solution was filtered through celite, and the solvent was removed under reduced pressure. The solid residue was redissolved in minimal THF (ca. 5 ml) and diluted with hexane (ca. 50 ml), until the solution started to turn cloudy. The solution was then swirled and left at −35 °C overnight to grow dark orange crystals of [(salNdipp)$_2$(DMAP)Os(^{15}NP)] (**3-^{15}N**). The mother liquor was removed by decanting, and the very dark orange crystals were washed with cold hexane 3×2 ml and dried under reduced pressure. Yield of [(salNdipp)$_2$(DMAP)Os(^{15}NP)] (**3-^{15}N**): 177.6 mg, 0.193 mmol, 94.1% based on (Bu_4N)[Os(^{15}N)Cl_4]. Crystals suitable for X-ray crystallography separated from a hexane solution of **3**, which was concentrated at −35 °C using toluene as sorbent. **^{31}P{^{1}H} NMR**, 161.99 MHz, C_6D_6, δ (ppm): 249.31 (**3**), 249.02 (**3-^{15}N**, $^1J_{PN}$ = 61.8 Hz). **^{15}N{^{1}H} NMR**, 81.11 MHz, C_6D_6, δ (ppm): 395.97 ($^1J_{NP}$ = 62.0 Hz). **IR**, solid between KBr windows, υ (cm^{-1}): 1258/1221 (P≡N) for **3**/**3-^{15}N**. **Elemental analysis**, calculated for $C_{45}H_{54}N_5O_2OsP$: C: 58.87%, H: 5.93%, N: 7.63%; found: C: 58.86%, H: 5.91%, N: 7.61%.

Synthesis of [(salNdipp)$_2$(DMAP)Os(NPS$_2$)] (4)

[(salNdipp)$_2$(DMAP)Os(NP)] (**3**, 25.0 mg, 27.2 μmol) and S_8 (1.74 mg, 54.3 μmol of S, 2.0 eq.)* were dissolved in 7.5 ml toluene, resulting in a slow color change from dark orange to dark green. The reaction mixture was cooled to −35 °C overnight, resulting in crystallization of [(salNdipp)$_2$(DMAP)Os(NPS$_2$)] (**4**) as dark orange crystals. The mother liquor was removed by decanting, and the dark orange crystals were washed with cold toluene (3×1 ml) and dried under reduced pressure. Yield of [(salNdipp)$_2$(DMAP)Os(NPS$_2$)] (**4**), 19.5 mg, 19.9 μmol 72.9% based on **3**. Crystals suitable for X-ray crystallography separated from the reaction mixture of [(salNdipp)$_2$(DMAP)Os(NPS$_2$)] (**4**). **^{31}P{^{1}H} NMR**, 243 MHz, THF-d_8, δ (ppm): 233.13 (**4**), 232.64 (**4-^{15}N**, d, $^1J_{PN}$ = 50.6 Hz). **^{1}H-^{15}N HMBC NMR**, 61 MHz, THF-d_8, δ (ppm): 954.53 (d, $^1J_{NP}$ = 50.5 Hz). **Elemental analysis**, calculated for $C_{45}H_{54}N_5O_2OsPS_2$: C: 55.02%, H: 5.54%, N: 7.13%; found: C: 54.74%, H: 5.59%, N: 7.05%.

** Note: Sulfur was weighed precisely by making a stock solution of 17.4 mg S_8 in 10 ml toluene and taking out a 1 ml aliquot.*

Synthesis of [(salNdipp)$_2$(DMAP)Os(NPCl)] (5)

[(salNdipp)$_2$(DMAP)Os(NP)] (**3**, 100.0 mg, 0.109 mmol) and Ph_3CCl (40.5 mg, 0.145 mmol, 1.3 eq.) were dissolved in 5 ml THF, and the reaction mixture was left for 3 hours. The solvent was removed under reduced pressure, and the dark orange residue was redissolved in a minimum amount of THF (3 ml), diluted with hexane (15 ml), cooled to −35 °C, and left to crystallize overnight. The mother liquor was removed by decanting, and the dark orange crystals of [(salNdipp)$_2$(DMAP)Os(NPCl)] (**5**) were washed with cold hexane (3×2 ml), and dried under reduced pressure. Yield of [(salNdipp)$_2$(DMAP)Os(NPCl)] (**5**): 100.7 mg, 0.106 mmol, 97.0% based on **3**. Crystals suitable for X-ray crystallography separated from a THF solution of [(salNdipp)$_2$(DMAP)Os(NPCl)] (**5**), with hexane/toluene as sorbent at −35 °C. **Magnetic moment**, μ_{eff} (Evans' method, THF-d_8, 298 K): 1.83 μ_B. **Elemental analysis**, calculated for $C_{45}H_{54}ClN_5O_2OsP$: C: 56.68%, H: 5.71%, N: 7.34%; found: C: 56.59%, H: 5.74%, N: 7.31%.

Synthesis of [(salNdipp)$_2$(DMAP)Os(η^1-N$_4$P)] (6)

[(salNdipp)$_2$(DMAP)Os(NPCl)] (**5**, 25.0 mg, 26.2 μmol) and Me_3SiN_3 (3.44 mg, 29.8 μmol, 1.15 eq) were dissolved in 1.5 ml THF, and the reaction mixture was left for 1 hour. The solution was diluted with hexane (ca. 10 ml) to precipitate out dark orange crystals of [(salNdipp)$_2$(DMAP)Os(η^1-N$_4$P)] (**6**), the mixture was cooled to −35 °C for 30 minutes and washed with 3×1 ml hexane. Yield of [(salNdipp)$_2$(DMAP)Os(η^1-N$_4$P)] (**6**), 13.9 mg, 14.5 μmol, 55.2% based on **5**. Crystals suitable for X-ray crystallography separated from a Et_2O solution of [(salNdipp)$_2$(DMAP)Os(η^1-N$_4$P)] (**6**), with toluene as sorbent at −35 °C. **Magnetic moment**, μ_{eff} (Evans' method, THF-d_8, 298 K): 1.85 μ_B. **Elemental analysis**, calculated for $C_{45}H_{54}N_8O_2OsP$: C: 56.29%, H: 5.67, N: 11.67; found: C: 53.68%, H: 5.83%, N: 11.45%; we attribute the sub-optimal elemental analysis to thermal decomposition of **6** during shipping.

*Note: other azide sources also convert **5** to **6**, but due to the low stability of the product, these methods do not allow a pure product to be isolated. **[1]** When using (Bu_4N)(N_3) in C_6D_6, **6** forms cleanly within 5 minutes, but the (Bu_4N)Cl byproduct has a similar solubility to **6**; attempts at removing (Bu_4N)Cl with alumina resulted in full decomposition of **6**. **[2]** When using NaN_3 in THF or dioxane, the formation of **6** is so slow that its thermal decomposition to **3** and N_2 complex **7** prevents isolation of a pure product. **[3]** When using NaN_3 with LiCl as phase-transfer catalyst in THF, the conversion rate is variable, and lithium ion remains in the sample, as verified from ^{7}Li NMR.*

Data Availability

All relevant data generated in this study, including full experimental procedures, crystal structures, magnetic data, ^{1}H, ^{13}C, ^{15}N, ^{31}P, COSY, HSQC, and 2D NMR data, IR, UV-vis, and XANES spectral data, as well as DFT calculations, are included in this Article and its Supplementary Information. Crystallographic data for structures reported in this Article have been deposited at the Cambridge Crystallographic Data Centre, under deposition numbers CCDC 2388538–2388544, which can be obtained free of charge via https://www.ccdc.cam.ac.uk/structures/.

Acknowledgements

A.R. thanks The Carlsberg Foundation (CF21-0438), The Swedish Research Council (2022-03154), The Royal Physiographical Society of Lund, Stiftelsen Lars Hiertas Minne (FO2022-0033), and The Crafoord Foundation (20230776) for funding. K.S.P. thanks The Carlsberg Foundation for a research infrastructure grant (CF17-0637). The authors thank the Danish Agency for Science, Technology, and Innovation for funding the instrument center "Danscatt". The X-ray spectroscopy experiments were performed at the ID12 beamline at the European Synchrotron Radiation Facility (Grenoble, France). The authors thank UTEP HPC JAKAR Cluster for the computational resources provided free of charge.

Author Contributions

All authors contributed to writing the manuscript and have approved the final version of it.

Competing Interests

The authors declare no competing interests.

Notes

Disclaimer: The views expressed are purely those of the authors and may not in any circumstances be regarded as stating an official position of the ERCEA and the European Commission.

Abbreviations

Bu = butyl, ^{t}Bu = *tert*-butyl, Me = methyl, OTf^{-} = triflate, Ph = phenyl, ^{i}Pr = *iso*-propyl, THF = tetrahydrofuran.

ORCID

Simon Edin 0000-0002-5759-1329
Christian Sandoval-Pauker 0000-0002-7831-331X
Nathan Yutronkie 0000-0002-8297-9376
Fabrice Wilhelm
Zoltan Takacs 0009-0009-8467-7265
Andrei Rogalev 0000-0002-0501-698X
Balazs Pinter
Kasper S. Pedersen 0000-0002-4381-4544
Anders Reinholdt 0000-0001-6637-8338